

Seismic performance evaluation of an infilled rocking wall frame structure through quasi-static cyclic testing

Pan Peng^{1†}, Wu Shoujun^{2‡}, Wang Haishen^{2‡} and Nie Xin^{1‡}

1. Key Laboratory of Civil Engineering Safety and Durability of China Education Ministry, Department of Civil Engineering, Tsinghua University, Beijing 100084, China

2. Department of Civil Engineering, Tsinghua University, Beijing 100084, China

Abstract: Earthquake investigations have illustrated that even code-compliant reinforced concrete frames may suffer from soft-story mechanism. This damage mode results in poor ductility and limited energy dissipation. Continuous components offer alternatives that may avoid such failures. A novel infilled rocking wall frame system is proposed that takes advantage of continuous component and rocking characteristics. Previous studies have investigated similar systems that combine a reinforced concrete frame and a wall with rocking behavior used. However, a large-scale experimental study of a reinforced concrete frame combined with a rocking wall has not been reported. In this study, a seismic performance evaluation of the newly proposed infilled rocking wall frame structure was conducted through quasi-static cyclic testing. Critical joints were designed and verified. Numerical models were established and calibrated to estimate frame shear forces. The results evaluation demonstrate that an infilled rocking wall frame can effectively avoid soft-story mechanisms. Capacity and initial stiffness are greatly improved and self-centering behavior is achieved with the help of the infilled rocking wall. Drift distribution becomes more uniform with height. Concrete cracks and damage occurs in desired areas. The infilled rocking wall frame offers a promising approach to achieving seismic resilience.

Keywords: infilled rocking wall frame; seismic performance; displacement distribution; quasi-static cyclic test

1 Introduction

Reinforced concrete (RC) frames are widely used around the world due to the clear load path, diverse plan layouts and satisfactory economic performance they provide. However, recent seismic hazard investigations involving both experimental and numerical analyses have demonstrated that this kind of structure system is prone to soft-story mechanism. The mechanism may lead to collapse, resulting in large casualties and economic losses (Doğangün, 2004; Goulet *et al.*, 2007; Haselton *et al.*, 2010; Zhao *et al.*, 2009). In soft-story mechanism, deformation is mostly concentrated in a single story, which results in poor structural behaviors (e.g., overall ductility, energy dissipation). Plastic hinges are formed at the ends of columns, rather than

beams. Moreover, even though a “strong column - weak beam” design philosophy is stipulated in most seismic design codes (CEN, 2004; ACI Committee 318, 2008; GB50011, 2010), soft-story mechanism may still occur due to several factors, including variations in material properties and the effect of a slab’s composition (e.g., thickness, strength). Even though RC frames may remain standing after an earthquake, excessive residual drift and severe damage to critical components make it difficult to retrofit, thus need to be demolished.

Rapid societal developments have increased the urgency of achieving earthquake resilience (Bruneau *et al.*, 2003). To realize this goal, seismic damage should be restricted to locations where critical load paths are not greatly affected. Specifically, in an RC frame structure, which may suffer from soft-story mechanism under severe earthquakes, a continuous component is expected to achieve uniform deformation along the height. Thus, a continuous component causes the RC frame to behave more predictably. It may also improve efficiency as well as facilitate the design of energy-dissipation devices.

In the study presented here, an infilled rocking wall is proposed as the continuous component in an RC frame structure. The structure system is therefore referred to as an “infilled rocking wall frame.” The rocking wall is described as “infilled” because it is built inside the frame, rather than outside of it. In conventional RC

Correspondence to: Nie Xin, Key Laboratory of Civil Engineering Safety and Durability of China Education Ministry, Department of Civil Engineering, Tsinghua University, Beijing 100084, China
Tel: +86-10-62794019; Fax: +86-10-62794019
E-mail: xinnie@tsinghua.edu.cn

[†]Professor; [‡]Graduate Student

Supported by: Natural Science Foundation of China under Grant Nos. 51178342 and 51578314

Received July 5, 2016; **Accepted** December 9, 2016

frames, infilled walls are mostly constructed with lightweight blocks, and functionalize as nonstructural partition components that undertake only self-weight. In design, infilled walls are represented as distributed loads on frame beams. Infilled rocking walls, however, are critical structural components in an infilled rocking wall frame. As the deformation mode is changed by the wall, interaction forces between the frame and the wall are large. For this reason, rocking walls should either be constructed with stiff blocks or cast directly from reinforced concrete. The infilled wall is described as “rocking” because the wall is not fixed to the foundation and can rotate around the bottom. As illustrated in Fig. 1, an infilled rocking wall is constructed with reinforced concrete continuously along the height of an RC frame. Frame columns adjacent to the wall are cut off at the bottom to allow uplift. With rocking characteristics, self-weight and vertical loads in the wall can be converted to self-centering forces that minimize residual drift. An infilled rocking wall provides a feasible approach to retrofitting an existing RC frame, which would otherwise be prone to soft-story mechanism in severe earthquakes due to a lack of uniform stiffness along the height.

Reinforced concrete frames associated with rocking-behavior walls have been researched in several studies. Alavi and Krawinkler (2004) compared the potential of fixed and pinned base walls to strengthen RC frames. When subjected to near-fault ground motions, the maximum demands on an RC frame can exceed codified values to a considerable degree, owing to the variability of earthquakes. Pinned walls were more effective in reducing drift demands and resulted in uniform story drift and better ductility. However, fixed walls were effective only in relatively stiff frames. Qu *et al.* (2012) investigated the application of a pin-supported wall in retrofitting an existing reinforced concrete frame. The concrete walls were arranged outside of the frame and connected to the foundation by hinges at the base. Nonlinear time-history analyses showed that this system performed satisfactorily in controlling deformation. Shear dampers were also introduced into the frame, and these

were shown to further reduce inter-story drift. Zibaei and Mokari (2014) numerically modeled controlled rocking walls in moment-resisting frames. Both concrete shear walls and rocking walls were considered. Compared with a shear wall, a rocking wall was found to achieve better uniformity in the frame. Ductility was better in the rocking system than in a system that used a bare frame or a shear wall frame. Weak-story mechanisms were removed without a significant change in the foundations. Concerning the distribution of inner forces, Pan *et al.* (2015) derived an analytical solution for a pin-supported frame wall structure using a distributed parameter model. Simplifications were made by regarding the frame and wall as shear beams and bending beams, respectively. Distributions of the displacements and inner forces relative to the stiffness of the wall and frame were achieved, and recommendations were made concerning desired wall stiffness.

In contrast to pin-supported walls, which are mostly arranged outside an RC frame, infilled rocking walls are built inside the frame in the proposed system. There are four main advantages to this system. First, an infilled rocking wall frame reduces undesirable restrictions on architectural layout. Lighting and visual field are not affected. Second, connections between rocking walls and frames can be simplified. In a pin-supported wall frame structure, shear forces between the frame and walls are transferred by connectors, requiring both large capacity and durability. Third, infilled walls are more convenient to construct, as they are arranged inside the frame. The proposed system is especially advantageous in retrofitting existing RC frames. Wall construction can be simplified by filling a frame with stiff bricks or reinforced concrete. The rocking characteristics are then achieved by cutting off base columns that are adjacent to the wall. Fourth, no additional enhancement is required to the frame foundation, because restraints at the bottom of the wall are released in a rocking wall.

An infilled rocking wall frame takes advantage of continuous component and rocking characteristics. Even though the satisfactory behavior of such a system can be anticipated by referring to similar structures, experimental study is valuable for detailed investigations of the proposed system prior to application in engineering practice. Critical components such as rocking joints at the base of walls and the intersection of walls and frames should be well-designed and tested. In this study, this seismic performance of an infilled rocking wall frame was investigated using quasi-static cyclic tests. For comparison, a conventional RC frame was constructed and tested under identical loading protocols. Capacity, stiffness, displacement, crack width, strain and the damage mode of the two systems were compared. The design and construction of critical joints were verified. Numerical models were built and calibrated, and frame shear forces in infilled rocking wall frames were estimated.

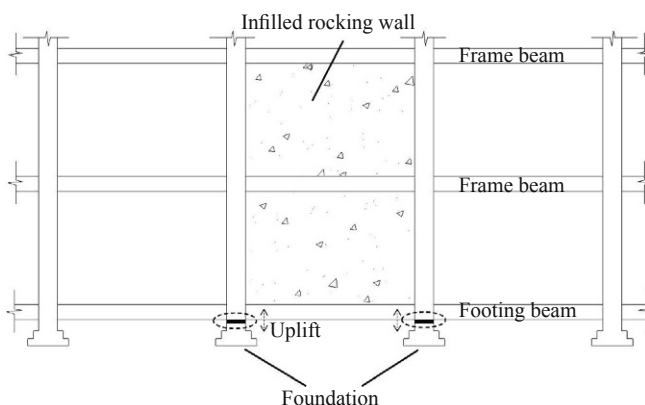


Fig. 1 Infilled rocking wall frame

2 Design of an infilled rocking wall frame

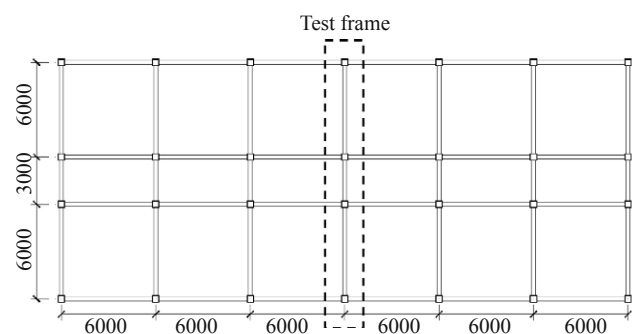
2.1 Prototype structure

To investigate the seismic performance of infilled rocking wall frame structure, an RC frame was designed following the current Chinese seismic design code (GB50011, 2010). The structure was located on a site with a seismic design intensity of 7.5 (the maximum spectrum acceleration was 0.12 g with a 50% probability of exceedance over a period of 50 years) and a site classification of II (with an equivalent shear-wave velocity between 200 m/s and 250 m/s for 20 m soil). Note that the prototype structure was placed in this location to facilitate a cyclic pushover test; an infilled rocking wall can be built in any location.

The structural plan is shown in Fig. 2. The prototype frame consisted of three stories, with each story being 3.6 m in height. The dead load and live load on the slab were 7 kN/m² and 2 kN/m², respectively. A concrete grade of C30 was used in frame beams, columns and rocking wall, with a nominal cubic compressive strength of 30 MPa. The longitudinal and transverse reinforcement steel grades were HRB335 (with a nominal yielding strength of 335 MPa) and HPB300 (nominal yielding strength 300 MPa), respectively. The cross-section was 500 by 250 mm in frame beams and 400 by 400 mm in frame columns.

2.2 Test model design

The middle frame, which is indicated notified by a dashed block in Fig. 2, was extracted and chosen for a testing. For comparison, both an infilled rocking wall frame and a conventional reinforced concrete frame were designed and constructed. Considering the loading capacity of actuators and the spatial limitations of the test site, two half-scale models were designed and cast in place. For brevity, the models are referred to as "the reinforced concrete frame model" (RCF model) and "the infilled rocking wall frame model" (IRWF model). The designs of the RCF and IRWF models are shown in Figs. 3(a) and 3(b), respectively. Both models were 5.4 m high, with 1.8 m in each story. Reinforcement in the models was obtained according to the prototype structure, with



Note: Dimensions in millimeters (mm)

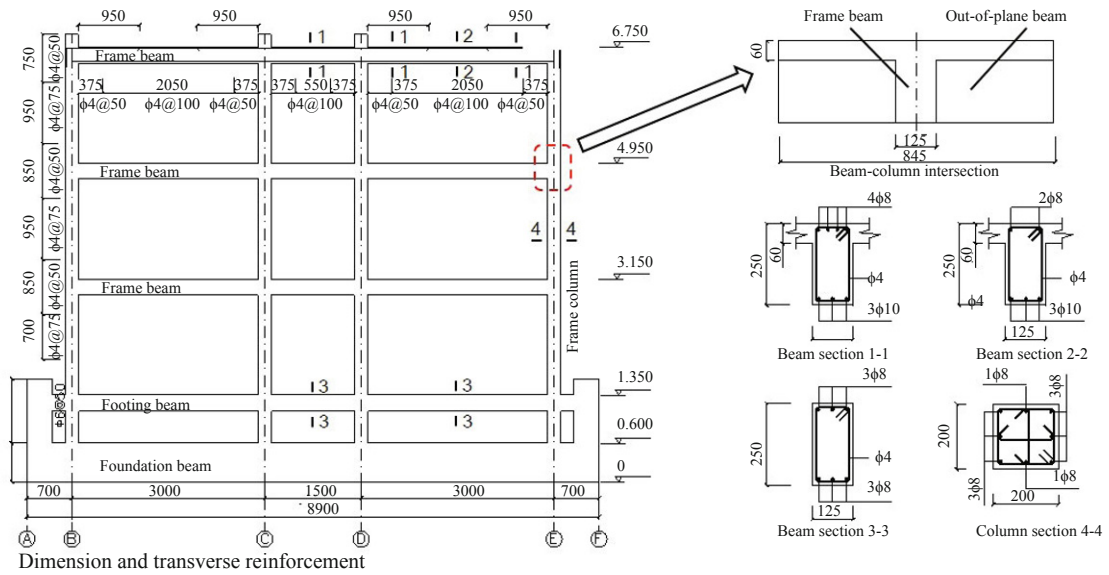
Fig. 2 Plan of prototype frame

a scaling factor taken into consideration. The diameters of the bars were 4, 6, 8 and 10 mm.

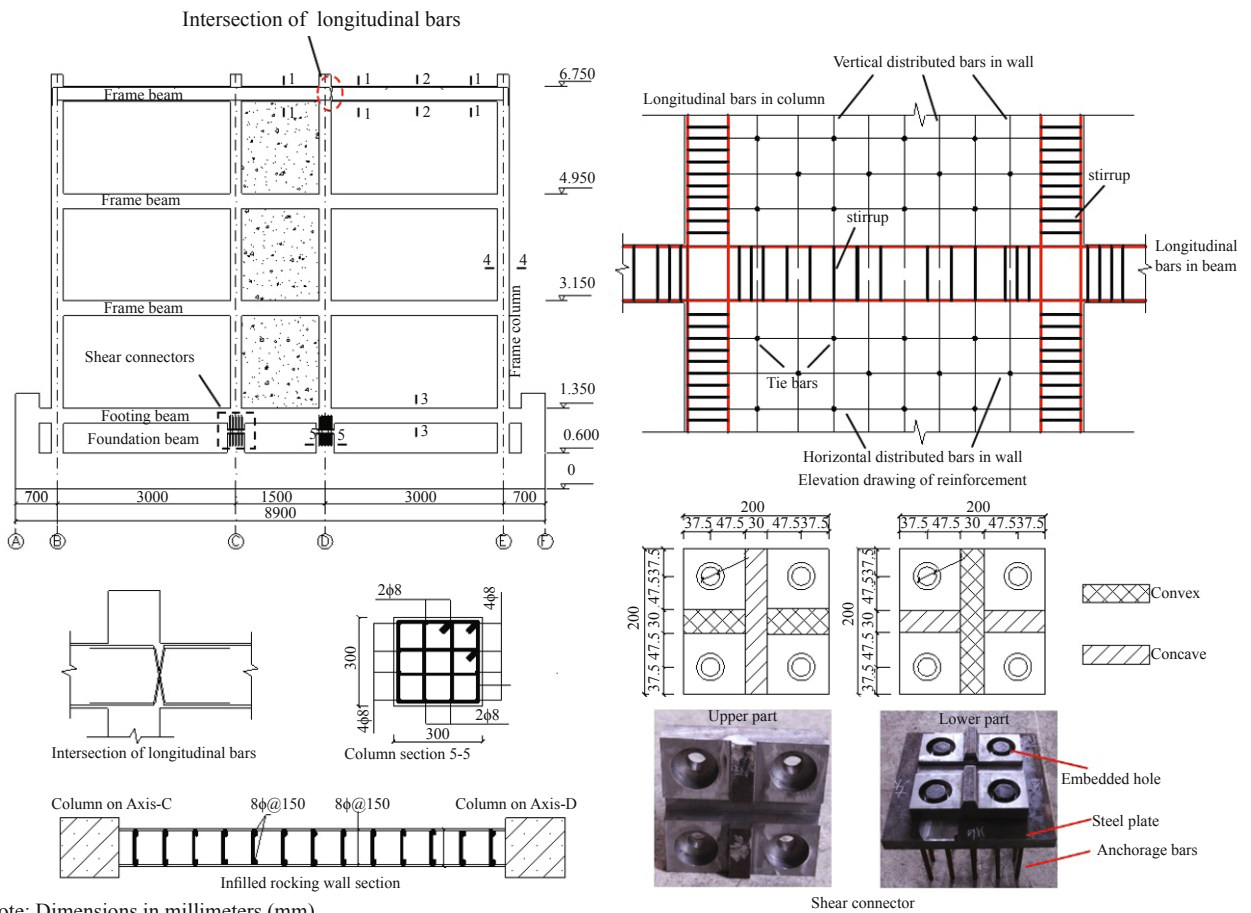
The RCF model's dimensions and transverse reinforcement are demonstrated in Fig. 3(a) on the left. Four frame columns were located on Axes B, C, D and E. The model was fixed to the ground by a foundation beam. The cross-section of foundation beam is 600 by 400 mm, much larger than the frame beams and columns. The reinforcement ratio in the foundation beam was sufficiently large to maintain elasticity during the entire loading process. To simulate boundary conditions in real structures, a footing beam was designed. The cross-section of footing beam was identical to the frame beams: 250 by 125 mm. The frame column was 200 by 200 mm in cross-section. As the negative moment was smaller, the longitudinal bars were cut off in the middle of frame beams between Axes B and C, as well as between Axes D and E. The longitudinal reinforcement of the frame beams is depicted in Fig. 3(a) on the right. To account for its influence on seismic performance, the slab was cast together with the frame beams. The slab thickness was 60 mm in the half-scale model, and its width was six times that of the slab thickness on both sides of the frame beams, in order to take into account stiffness contribution to the connected beam (GB50010, 2010). Out-of-plane beams were also built. The cross-section of the out-of-plane beams was the same as that of the frame beams, and their lengths were equal to that of the slab width.

As illustrated in Fig. 3(b), the IRWF model's dimensions and longitudinal and transverse reinforcement were almost identical to those of the RCF model. The IRWF model differed from the RCF model in three ways: First, the model was reinforced differently at the frame beam-column joint on Axis D in Story 3. The longitudinal bars at the top and bottom of the beam intersected in the middle of the beam section. This design anticipated that the beam ends connected to the wall would experience substantial deformation as the wall rocked. The intersection was constructed to enhance the deformation abilities of the beam-column joints, which were crucial for shear transfer between the frame and the wall. For comparison, the beam-column joints in Stories 1 and 2 and on Axis C in Story 3 remained the same as in the RCF model. Second, the frame columns on Axes C and D were cut off at the bottom. The cross-section of the columns was 300 by 300 mm under the footing beam to enable the construction of shear connectors. Third, an infilled rocking wall was constructed. The thickness of the wall was 125 mm. Distributed bars in the wall complied with the minimum reinforcement and maximum spacing required in a shear wall (GB50010, 2010). Tie bars were used to strengthen the connection between the two rebar layers in the wall.

To ensure rocking behavior and to restrain in-plane and out-of-plane sliding of the wall, shear connectors at the bottom of the rocking wall were designed. Each shear connector consisted of upper and lower parts. In each



(a) RCF model



(b) IRWF model

Fig. 3 Design of test models

part, there were both convex and concave structures. The structural dimensions were designed to ensure interlocking under the allowable value of manufacturing errors. Each part of the shear connector was connected to a steel plate by bolts through four embedded holes. The steel plate was then anchored to a concrete column by bars. The dimensions and anchorage of the shear

connectors were checked to ensure sufficient shear capacity during the loading process.

2.3 Material properties

The RCF and IRWF models were both cast in place. One story (including the foundation and footing beams)

was cast at a time. The average time interval between the construction of adjacent stories was seven days. To better simulate the rocking wall's retrofitted structure, frame beams and columns were also cast in the IRWF model. For the sake of time, the rocking wall was cast at the same time as the frame beams and columns. Concrete cube samples were cast in each cast. Both the RCF and IRWF models were cured for 28 days after cast of story 3 before quasi-static cyclic testing was initiated.

Material properties were tested in accordance with GB50010 (2010). Compressive tests on concrete samples were carried out on the same day as the pushover tests. Tables 1 and 2 summarize the mechanical properties of the concrete and steel, respectively. In Table 1, $f_{cu,m}$ denotes the mean value of the compressive strength of the cubic concrete samples with dimensions of 100 by 100 by 100 mm, and $f_{c,m}$ represents the axial compressive strength, which is used in the numerical models. The relationship between $f_{cu,m}$ and $f_{c,m}$ is $f_{c,m} = 0.76 f_{cu,m}$. In Table 2, $f_{y,m}$ denotes the yielding strength of reinforcement steel, $f_{u,m}$ is the ultimate strength, and E is Young's modulus.

3 Test setup

3.1 Loading facilities

Figure 4 summarizes the setup of the quasi-static cyclic tests. The models were arranged in a west–east direction. The axial load was imposed by two vertical actuators, VA1 and VA2, which were located in the same plane at the top of the models. Two distribution beams were placed at the top of the frame columns. The position of the actuator on the distribution beams was based on the axial force ratio of the middle and side columns. The axial force ratio is defined as:

$$n = \frac{N}{f_c A_c} \quad (1)$$

where N denotes the axial forces applied on the column, and f_c and A_c denote the compressive strength of the column's concrete and cross-sectional area, respectively. The axial force ratios in the side and middle columns were 0.21 and 0.15, where the standard concrete compressive strength was 30 MPa. The ratios were identical in design under both dead and live loads.

Test models were subjected to lateral forces by three horizontal actuators at each story level, HA1, HA2 and HA3. To better impose cyclic loads, two loading tendons with steel plates on both ends were installed, and the horizontal actuators were connected to them. To avoid out-of-plane movement, four pairs of steel supports were installed to clip the model to restrict horizontal slippage. Two screw jacks were used to fix the foundation beam. The foundation beams were further anchored by anchor bolts to the strong floor.

3.2 Loading protocol

During quasi-static cyclic tests, the axial force at both vertical actuators, VA1 and VA2, was 430 kN. With the help of distribution beams, the axial forces imposed on middle columns and side columns were 248 and 182 kN, respectively. The horizontal force at the actuators

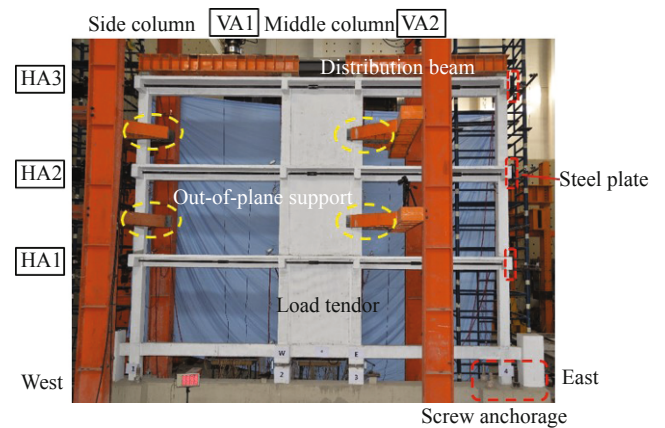


Fig. 4 Test setup

Table 1 Mechanical properties of concrete

Model	RCF		IRWF	
	$f_{cu,m}$ (MPa)	$f_{c,m}$ (MPa)	$f_{cu,m}$ (MPa)	$f_{c,m}$ (MPa)
Location				
Foundation beam	45.70	34.73	47.12	35.81
Footing beam	43.47	33.03	39.05	29.68
Story 1	39.75	30.21	27.29	20.74
Story 2	31.41	23.87	27.97	21.26
Story 3	38.64	29.36	37.81	28.73

Table 2 Mechanical properties of steel

Diameter (mm)	$f_{y,m}$ (MPa)	$f_{u,m}$ (MPa)	E (MPa)
4	254.65	366.06	187735
6	364.17	641.57	194996
8	335.29	630.98	194492
10	320.35	756.32	191924

followed an inverted triangular distribution; i.e., the axial loads in HA1, HA2 and HA3 were proportioned 3:2:1. Meanwhile, loading was controlled by horizontal displacement in Story 3 (top displacement) by actuator HA3. Positive loading was arbitrarily defined as pushing towards the east, while negative loading was pulling towards the west. For a detailed realization of the loading algorithm, refer to Pan *et al.* (2014). The loading path is shown in Fig. 5. Top displacement varied from 0.0054 to 0.108 m, which corresponds to a structural drift angle θ (top displacement divided by the structural height) of 1/550 to 1/50. There were seven amplitudes in total, and each amplitude was loaded for three cycles.

3.3 Data acquisition

Figure 6 shows the data acquisition facilities in the IRWF model. Strain gauges were attached in longitudinal bars within frame beams and columns. The gauges located near beam-column intersections, where plastic strain might be large. Six transducers, H11, H12, H21, H22, H31, and H32, were used to measure horizontal displacements. Two transducers in each story were deployed for calibration. The transducers were fixed on a scaffold and connected to the frame by metal wire. Two transducers, V1 and V2, were arranged at the bottom of footing beam near Axes C and D to measure uplift in the rocking wall. External horizontal forces were achieved

by actuators HA1, HA2 and HA3. For simplicity, the four columns were labeled 1 to 4 from west to east. Note that data acquisition facilities in the RCF model were similar to those in the IRWF model, except that V1 and V2 were removed.

4 Results and discussion

4.1 Hysteretic behavior

Hysteresis loops for the IRWF and RCF models are shown in Figs. 7(a) and (b), respectively. The x axis denotes top displacement, while the y axis denotes base shear forces. Note that base shear forces were achieved by summing up axial loads in three horizontal actuators. As base shear forces differed substantially in the two models, different y -scales were applied for clarity.

The IRWF model showed clear self-centering characteristics. Even though the structural drift ratio reached 1/50, residual drift was almost negligible when the base shear force returned 0. There are two reasons for the IRWF model’s self-centering behavior. First, the axial forces in the two vertical actuators applied self-centering moment. Second, damage in the IRWF model was limited; this is discussed in Section 4.4. In the RCF model, however, residual drift was quite obvious, even at a small drift. When the structural drift ratio θ , residual drift was 6.6 mm. Larger loading amplitude resulted in larger residual drift. Axial forces in the vertical actuators and the model gravity tended to prevent the frame from returning to its original location. Thus, with its satisfactory self-centering behavior, the IRWF model demonstrated better seismic resilience over the RCF model, since residual drift is a critical factor for retrofit feasibility and downtime. $\theta = 1/100$.

4.2 Stiffness and capacity

Since obvious stiffness degradation occurs at skeleton curves, yielding points were determined according to skeleton curves. The skeleton curves achieved from hysteresis loops are demonstrated by dotted lines with

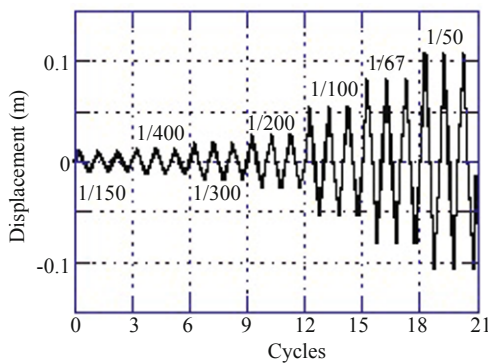


Fig. 5 Loading path in Story 3

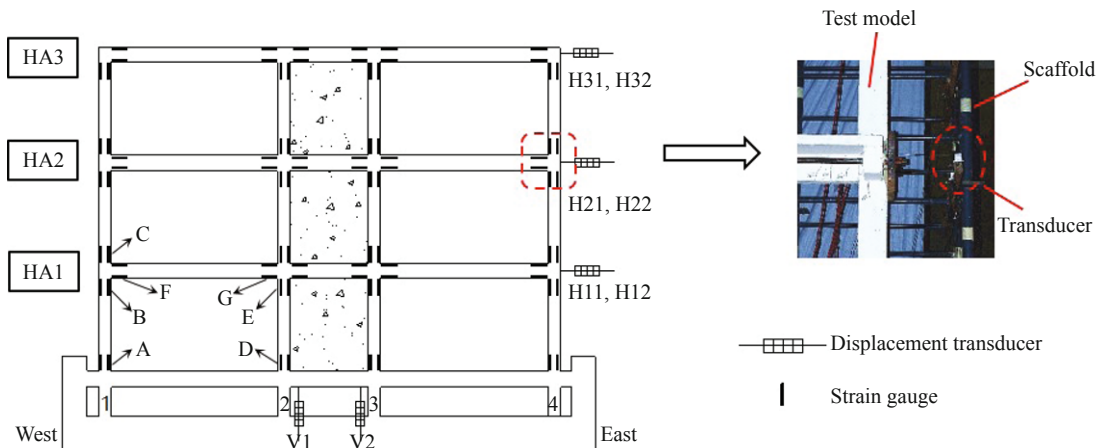


Fig. 6 Data-acquisition facilities

circular marks in Figs. 7 (a) and 7(b), respectively. Each dot represents an amplitude. Critical data are listed in Table 3. The skeleton curve for the IRWF model can be divided into three stages.

(1) Before the wall rocked: When the structural drift angle θ was less than 1/400, the two parts of the shear connectors at the bottom of the rocking wall remained in contact. As no uplift occurred, the wall in the IRWF model behaved as a conventional shear wall. The initial stiffness was 20.03 kN/mm in the IRWF model, compared with 7.38 kN/mm in the RCF model, more than 1.7 times larger. The large cross-section of the rocking wall contributed to its high initial stiffness.

(2) After the wall rocked but before the frame yielded. The wall began to rock when the structural drift angle exceeded 1/400. Stiffness degraded in the IRWF model, but remained almost identical during successive loading until the frame yielded.

(3) After the frame yielded. The frame in the IRWF

model yielded at a structural drift ratio of 1/200. The RCF model yielded at a much smaller amplitude, when the structural drift ratio was 1/400.

Even though reinforcement in the frame columns and beams was almost identical, shear capacity was greatly improved in the IRWF model over the RCF model. The peak base shear force in the IRWF model was 321.0 kN, more than twice than in the RCF model, 155.3 kN. Two reasons account for this incremental difference in base shear force. First, in the IRWF model, axial forces at the vertical actuators helped to resist horizontal loads as the wall rocked. In contrast, in the RCF model, vertical loads contributed little to resisting horizontal load, since the frame columns were fixed to the foundation beam. Second, the rocking of the wall amplified the deformation of the frame beams that were connected to it, thereby increasing the resisting moment in the model. Both models showed a slight capacity degradation when the structural drift ratio θ reached 1/50.

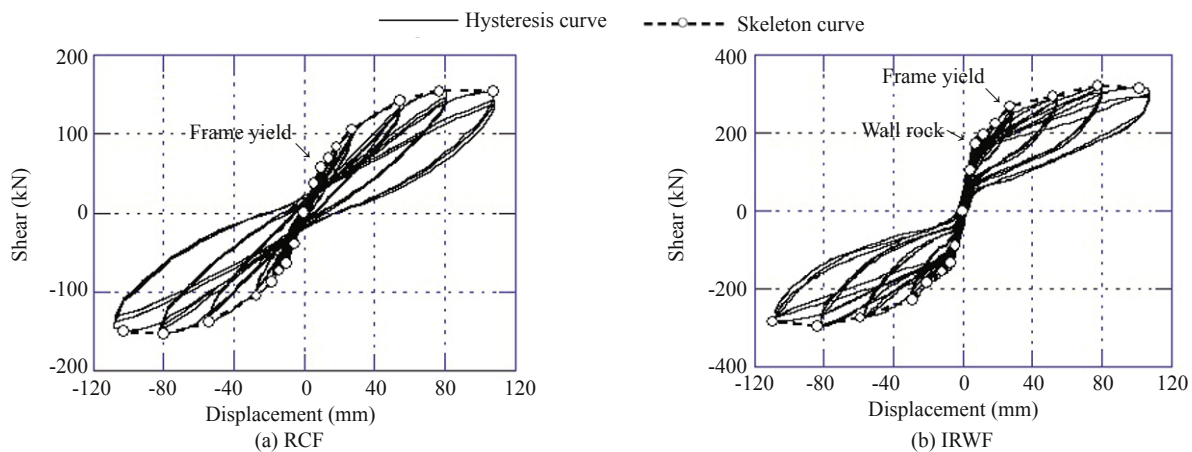


Fig. 7 Hysteresis loop and skeleton curve

Table 3 Comparison of the two models

Model	Initial stiffness (kN/mm)	Shear capacity (kN)	Yielding drift ratio	Capacity degradation drift ratio
RCF	7.38	155.3	1/400	1/50
IRWF	20.03	321.0	1/200	1/50

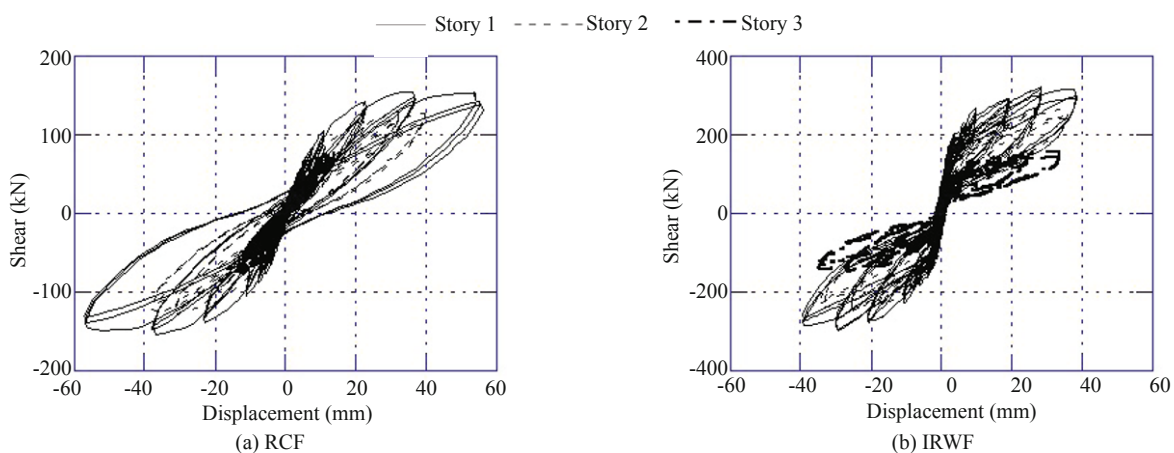


Fig. 8 Hysteresis loop in each story

4.3 Inter-story drift

Figures 8 (a) and 8 (b) show hysteresis loops for the three stories in the RCF and IRWF models, respectively. In the figure, the x axis represents inter-story drift, which is the displacement difference between the horizontal transducers in the two stories. The y axis represents story shear force, calculated by summing the axial forces in horizontal actuators. The shape of the hysteresis loops was similar in the three stories. However, inter-story drift differed substantially. In the RCF model, inter-story drift at amplitude 1/50 was 57.2, 39.8 and 13.9 mm in the three stories, respectively. Drift in Story 1 was more than 50% of top displacement. The severe drift concentration that occurred in Story 1 could result in collapse in a real structure. The corresponding inter-story drifts in the IRWF model was 39.3, 35.7 and 34.7 mm, respectively. The infilled rocking wall behaved as a continuous component, forcing the frame to deform uniformly along the height. This characteristic can improve the efficiency of energy dissipation devices, especially displacement dependent devices, such as buckling restraint braces and friction dampers. Thanks to the infilled rocking wall, the performance of the RC frame became more predictable and displacement concentration in the bottom story was avoided.

4.4 Crack width and damage distribution

In addition to residual drift, damage is another factor that affects earthquake resilience. Concrete cracks provide an index to directly measure damage in RC structures. Figure 9 compares two models' maximum crack width corresponding to each amplitude in Story 1. Three components were considered: frame beam, frame column and footing beam (refer to Fig. 3). Note that the maximum crack width denotes the maximum value in the three cycles for each amplitude. When concrete spalling occurred, a crack width of 4.0 mm was assigned for simplification. Crack widths after tests were also measured, corresponding to amplitude 0 at the end of the x axis.

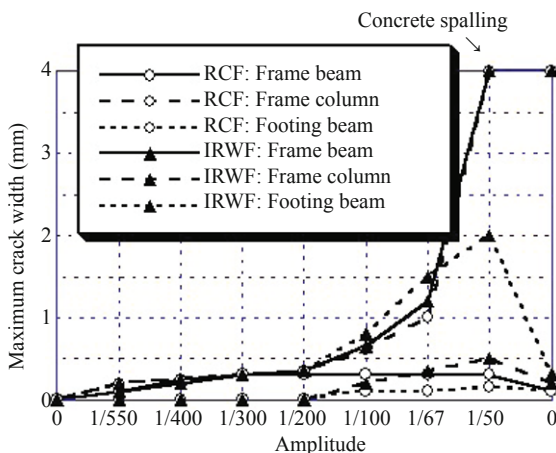


Fig. 9 Crack width development

The two models demonstrate evident differences in crack development. In the RCF model, concrete crack appeared in the frame beam at amplitude 1/550. Cracks in the frame beam and column developed synchronously with the increase in width. The footing beam began to crack at amplitude 1/200. Crack distribution developed further in the frame and footing beams, but the maximum width remained constant until the end of the test. In contrast, the maximum crack continued to increase in the frame column after amplitude 1/200. At amplitude 1/67, concrete in the frame column crushed near the two ends. During the three cycles at amplitude 1/50, concrete spalling became increasingly severe. The spalling was concentrated at column ends, and especially at the base. In conclusion, concrete damage gradually changed from being distributed in the whole model to concentrating in the frame columns. As demonstrated in Fig. 7, capacity degraded at amplitude 1/50.

In the IRWF model, concrete cracked in the footing beams at amplitude 1/550, as well as in the frame columns and beams. Crack distribution developed and maximum width increased with amplitude. The maximum width in the frame beam and column was less than that in the RCF model. The maximum width in the footing beam remained greater than in the frame beam and column during the test. At amplitude 1/67, the maximum crack widths in the frame beam, column and footing beam were 1.2, 1.5 and 0.6 mm, respectively. Concrete spalling occurred at amplitude 1/50 in the frame beams at the ends that were connected to the infilled rocking wall. Crack width increased further in the frame column and footing beams, but distribution remained almost constant. After the test, the frame column and footing beam returned to the original locations, and crack width became relatively small (0.25 and 0.2 mm, respectively). In conclusion, limited damage was initially widely distributed in the IRWF model. Damage gradually concentrated in the frame beams at large amplitudes.

Figure 10 shows crack distribution after the test in the side column, middle column and beam-column intersections in Story 1. Two colors are used in the crack notation. Red lines represent cracks that developed during the positive loading (to the west), while black lines represent crack developed with negative loading (to the east). In the RCF frame near the intersection of the frame column and footing beam (Figs. 10 (a) and 10 (b)), most cracks were formed at the base of the middle and side columns. The footing beam did not crack until amplitude 1/100. Figure 10(c) illustrates the crack distribution near the intersection of the frame column and frame beam. Cracks were distributed more widely in the frame beam than in the frame column. Although cracks first appeared in the frame beam at amplitude 1/550, it was at the column base and top where concrete spalled. Buckling of longitudinal bars appeared at the bottom of the middle column, where plastic hinges formed.

For the IRWF model, Figs. 10 (d) and 10(e) illustrates a wider crack distribution in the footing beam than at the

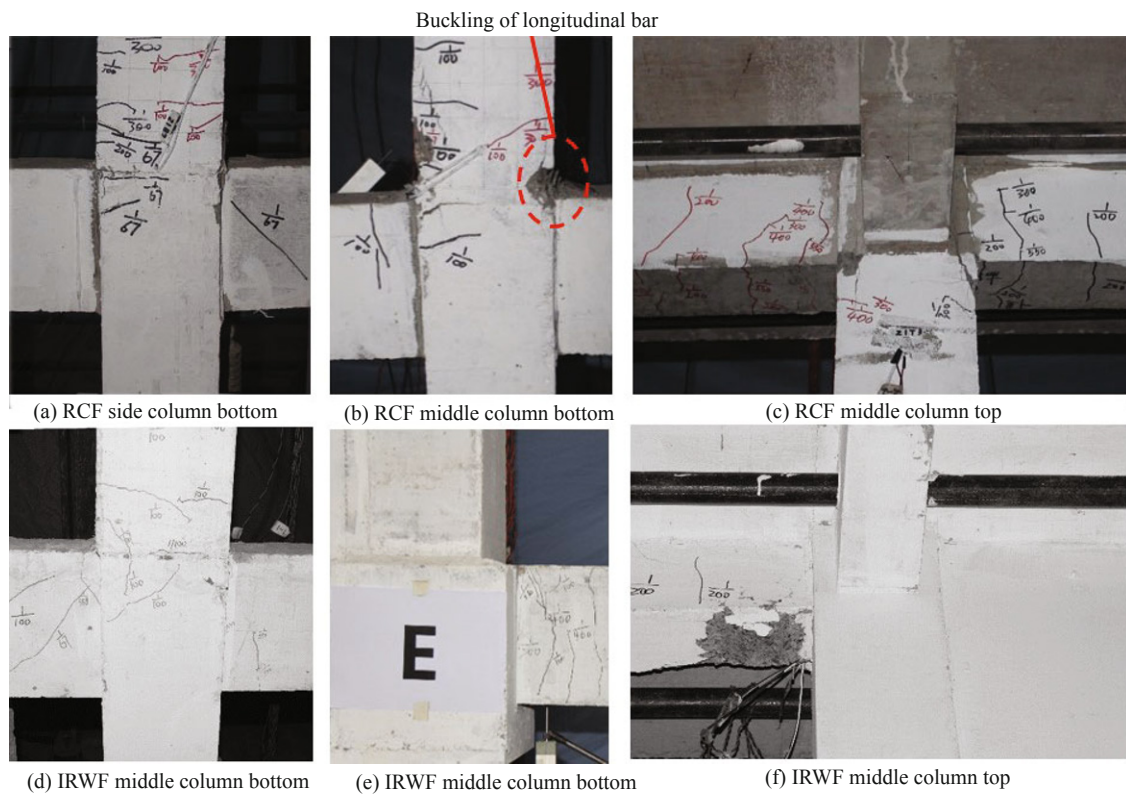


Fig. 10 Damage mode

base of the frame column. Specifically, the end of the footing beam that was connected to the middle column (rocking wall) cracked more severely than the end that was connected to the side column. No crack formed at the bottom or top of the side column until amplitude 1/100. In the middle column, which was adjacent to the rocking wall, no visible damage appeared during the test (Figs. 10 (e) and 10 (f)). Concrete spalling at amplitude 1/50 was concentrated at the intersection of the frame beam and middle column (rocking wall), as illustrated in Fig. 10 (f). Note that the slab cracked at amplitude 1/100; the 10.5 mm wide crack is located above the spalling frame beam in Fig. 10 (f). Therefore, special construction should be designed for the slab that is adjacent to a rocking wall, aiming at improving deformation ability.

Based on crack and damage development in the RCF model, even a code-compliant RC frame—built using a strong column–weak beam hierarchy that has been ensured by an amplification coefficient—may still deteriorate due to soft-story mechanism. In an RC frame structure, columns are a critical component for gravity transfer. Damage to columns may degrade capacity and incur large residual drift. Collapse may even occur as a result of large lateral displacement. Comparatively, beams are not as critical as columns, and a uniform distribution of beam hinges may be expected to achieve satisfactory energy dissipation. As shown in the IRWF model, an infilled rocking wall provides a promising approach for transferring the damage mode from column hinges to beam hinges, thus avoiding soft-story mechanism and resulting in large energy dissipation.

4.5 Rocking joint uplift and intersection damage

Figure 11(a) depicts the uplift of a rocking joint at the base of the middle column at amplitude 1/50 during negative loading. No relative horizontal displacement was observed in the shear connector, which confirms the validity of the restraining function. Figure 11(b) shows the uplift and top displacement at each amplitude. The uplift, represented by a continuous line with circles, was measured by vertical transducer V2 (annotated in Fig. 6). The top displacement, measured by transducers H31 and H32 in Story 3, is annotated by a dashed line with triangles. The rocking joint began to uplift at amplitude 1/400, which is consistent with the skeleton curve in Fig. 7. Before amplitude 1/100, the uplift increased almost proportionally with top displacement. The rocking wall behaved as a rigid body. The uplift increment became a little slower than top displacement after amplitude 1/100, which resulted from self-deformation of the wall.

Figure 12 demonstrates the damage mode of the frame beam–column intersections in the IRWF model after the test for clarity. The location of each connection is annotated in the upper figure. Concrete spalling was mostly concentrated in the intersections of the frame beam and middle column, while the intersections of the frame beam and side column suffered less. As introduced in Section 2.2, longitudinal bars intersected in the frame beam, which was connected to the middle column in Story 3. Specifically in the intersection (i), concrete spalling damage was evidently alleviated, thereby validating the purpose of the design.

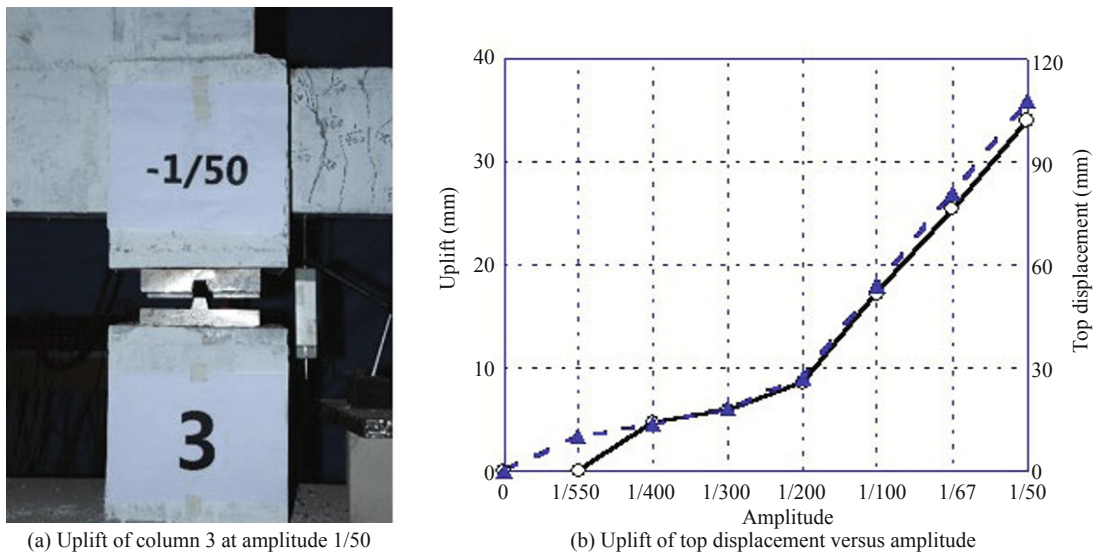


Fig. 11 Uplift of rocking joint

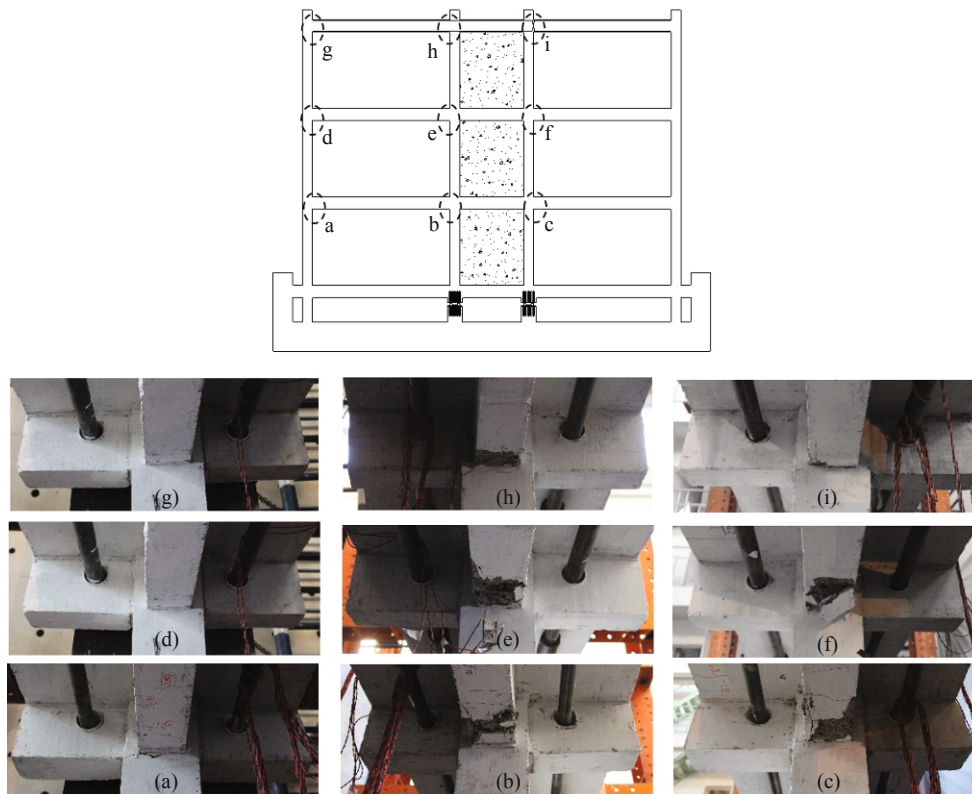


Fig. 12 Damage mode of beam-column intersection in the IRWF model

4.6 Strain development

Steel strain indicates the development of plasticity in a local area. Strain development in seven gauges is demonstrated in Fig. 13. The locations of the gauges are annotated in Figure 6. Gauges A, B, C, D and E were arranged on longitudinal bars in frame columns. Among them, Gauges A and B were at the top and bottom of Column 1 (side column) in Story 1, while gauge C was located at the bottom of Column 1 in Story 2. Gauges D and E were at the top and bottom of Column 2 (middle column) in Story 1. Gauges F and G were arranged on

longitudinal bars in the frame beam in Story 1 near two ends.

Figure 13(a) shows that strain in the columns and beams in the RCF model increased synchronously until amplitude 1/200. After that, strain developed much faster in the columns than in the beams. A comparison of Gauges A and B or D and E shows that steel strain was greater in column's base than in its top. A comparison of Gauges A and C indicates that plasticity at the column base was larger in Story 1 than Story 2. In particular, strain in Gauge A increased almost linearly after amplitude 1/200, while the increment in Gauge C was much smaller.

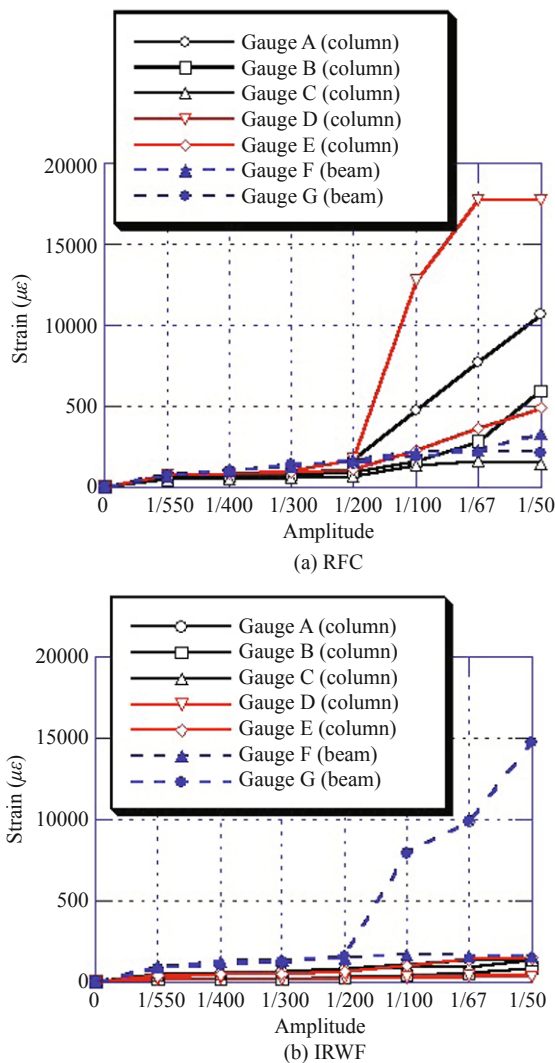


Fig. 13 Strain development in frame beam and column

After amplitude 1/67, strain even decreased in Gauge C. Strain in Gauge E increased greatly after amplitude 1/100, indicating severe damage at the base of Column 2, which is consistent with the damage mode shown in Figure 10(b). Strain in the frame beam (Gauges F and G) was smaller than in the columns. Even at amplitude 1/50, longitudinal bars were just beyond yielding.

According to Figure 13(b), strain development in a frame column in the IRWF model was moderate. Maximum strain in a frame column was much smaller than in the RCF model. Similar to the RCF model, column strain at the base was greater than at the top. A comparison of Gauges A and C shows that strain at the column base in Stories 1 and 2 was almost identical, which indicates similar deformation. Even at amplitude 1/50, longitudinal bars in the frame column did not yield. This is a preferred situation, as quite limited damage was accumulated in the frame column, a critical component in a RC frame. Different from the RCF model, the maximum strain appeared in the beam rather than in the column. A comparison of Gauges F and G shows that more plasticity was accumulated at beam ends that were connected to middle columns (rocking wall). Therefore,

to improve the behavior of IRWF systems, sufficient attention should be focused on the proper design of connections between the frame beam and rocking wall.

5 Estimation of shear forces in frames

5.1 Finite element modeling

Generally speaking, an experimental measure of shear forces in a reinforced concrete frame is not convenient or accurate. To investigate frame column shear forces in an IRWF model, finite element models were built in OpenSees (Mazzoni *et al.*, 2006) and calibrated according to hysteresis loops. Figure 14 demonstrates a schematic element partition and boundary conditions for an IRWF model. In the model, concrete and steel materials were modeled by Concrete01 and Steel02, respectively. Confined concrete was represented by a Saatcioglu-Razvi model that take into consider increments of strength and ductility due to stirrup (Saatcioglu and Razvi, 1992). The residual strength was taken to be 0.2 times that of peak strength. Nodes were defined at the intersections of beams and columns, as well as places where stirrup spacing changed. Displacement-based beam-column elements were used to model beams and columns. The P-Delta effect was taken into consideration in the columns. As demonstrated by the damage mode and strain gauges, no evident damage was observed in the infilled rocking wall. Therefore, elastic shell elements were used to model the infilled rocking wall. Shear connectors at the bottom of the wall were modeled by elastic no-tension elements. Compressive stiffness was given a relatively large value. Translational movement in the x axis was restricted at the bottom of the wall to simulate the effect of shear connectors on restraining the relative in-plane displacement between the wall and the base. Out-of-plane translations of the frame and the wall were restrained. Finite element modeling of the RCF

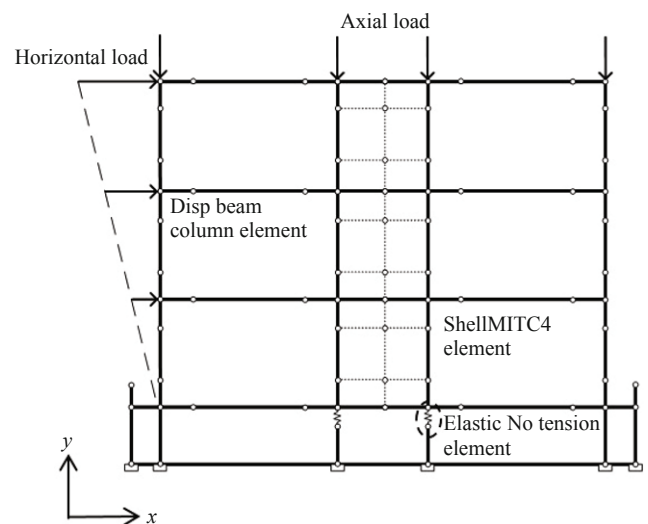


Fig. 14 Element definition and boundary conditions in IRWF model

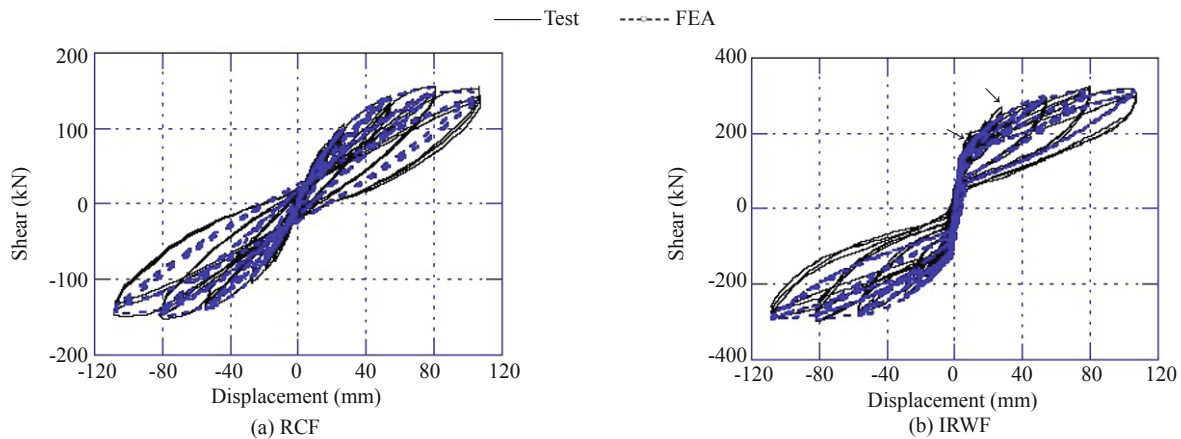


Fig. 15 Comparison of hysteresis loop

model was similar to that of the IRWF model, without modeling rocking joints or the wall.

5.2 Shear forces in the frame of an IRWF model

Figure 15 demonstrates the hysteresis loops produced by the two models. The x axis denotes the top displacement and Y axis denotes base shear forces. Results from the numerical model match well with the hysteresis loop of the RCF model, which indicates that frame beam and column modeling are feasible. Finite element modeling of the IRWF model also indicates high accuracy. Error in unloading was greater than in loading; this may have been caused by variations of vertical axial forces in the actuators as the wall rocked during the test. In general, it is reasonable to estimate shear forces according to the numerical model.

Figure 16 shows shear force in frame columns at each amplitude for the IRWF model. Frame shear forces were calculated by summing up shear forces in Columns 1 and 4 in each story. Frame shear forces were almost identical at relatively small amplitudes. Although the difference became slightly greater at larger amplitudes, frame shear forces still matched well across the three stories, which explains the uniform displacement distribution in the IRWF model.

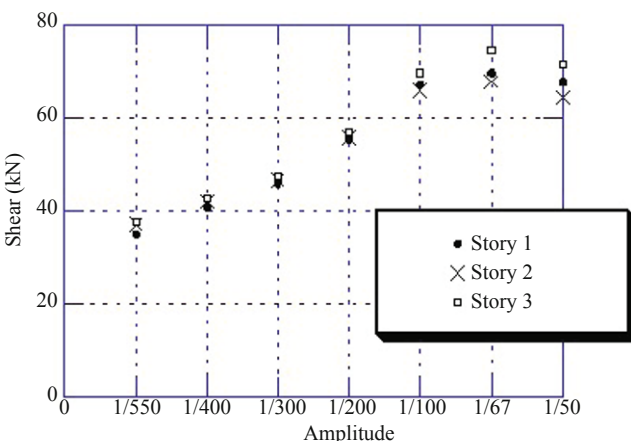


Fig. 16 Frame shear forces in IRWF model

6 Conclusions

This paper proposes a novel structure system, an infilled rocking wall frame structure, in which the rocking wall behaves as a continuous component. In the system, rocking walls are embedded in a frame, which facilitates wall construction and avoids complexity in frame-wall connection. The seismic performance of the proposed system was investigated through a quasi-static cyclic test. For comparison, a reinforced concrete frame (RCF) model and an infilled rocking wall frame (IRWF) model were designed faithfully following Chinese seismic design codes. The contributions of slabs, out-of-plane beams, and footing beams were considered. Comparisons on capacity, stiffness, displacement, crack width, strain and damage mode were made. Critical joints were designed and verified. Finite element models were built and calibrated, and column shear forces in the IRWF model were achieved and compared. The main conclusions are as follows.

(1) Capacity and initial stiffness are evidently improved in the IRWF model, with capacity at more than 2 times and initial stiffness at 2.7 times that of the RCF model. The IRWF model also demonstrated satisfactory self-centering ability and negligible residual drift.

(2) The rocking wall has promising control on displacement distribution. Inter-story drift remained uniform along the height. When the structural drift ratio was 1/50, drift was 39.3, 35.7 and 34.7 mm for the three stories, respectively.

(3) The code-compliant RC frame may suffer from soft-story failure. In the RCF model, drift in Story 1 was more than 50% of the total displacement.

(4) Soft-story mechanism was avoided in the IRWF model. Damage and plastic hinges were concentrated in the frame beam rather than in the frame column, indicating better ductility and energy dissipation.

(5) Performance of the IRWF model verified the design and feasibility of critical joints. Shear connectors restricted in-plane movement of the rocking wall at its base, while releasing vertical constraints to facilitate rocking behavior. Intersect construction in the frame

beam improved its deformation ability.

(6) The numerical model matched well with test results. Similar frame shear forces for all three stories explain the uniform displacement distribution in the IRWF model.

(7) The infilled rocking wall frame provides a promising approach for improving seismic performance and achieve resilience in RC frames.

Acknowledgment

The authors gratefully acknowledge the financial support of the Natural Science Foundation of China under Grant No. 51178342 and 51578314.

References

- ACI Committee 318 (2008), Building Code Requirements for Structural Concrete (ACI 318-08) and Commentary (ACI 318R-08), American Concrete Institute, Farmington Hills, MI.
- Alavi B and Krawinkler H (2004), “Strengthening of Moment-resisting Frame Structures Against Near-Fault Ground Motion Effects,” *Earthquake Engineering & Structural Dynamics*, **33**(6): 707–722.
- Bruneau M, Chang SE, Eguchi RT, Lee GC, O’Rourke TD, Reinhorn AM, Shinozuka M, Tierney K, Wallace WA and Winterfeldt Dv (2003), “A Framework to Quantitatively Assess and Enhance the Seismic Resilience of Communities,” *Earthquake Spectra*, **19**(4): 733–752.
- CEN (2004), *Eurocode 2-Design of Concrete Structures Part 1-1: General Rules and Rules for Buildings, EN-1992-1-1:2004 E*, Comite Europeen de Normalization, Brussels, Belgium.
- Doğangün A (2004), “Performance of Reinforced Concrete Buildings during the May 1, 2003 Bingöl Earthquake in Turkey,” *Engineering Structures*, **26**(6): 841–856.
- GB50010-2010 (2010), *Code for Concrete Design of Structure*, Beijing: China Building Industry Press. (in Chinese)
- GB50011-2010 (2010), *Code for Seismic Design of Buildings*, Beijing: China Building Industry Press. (in Chinese)
- Goulet CA, Haselton CB, Mitrani-Reiser J, Beck JL, Deierlein GG, Porter KA and Stewart JP (2007), “Evaluation of the Seismic Performance of a Code-Conforming Reinforced-concrete Frame Building—from Seismic Hazard to Collapse Safety and Economic Losses,” *Earthquake Engineering & Structural Dynamics*, **36**(13): 1973–1997.
- Haselton CB, Liel AB, Deierlein GG, Dean BS and Chou JH (2010), “Seismic Collapse Safety of Reinforced Concrete Buildings. I: Assessment of Ductile Moment Frames,” *Journal of Structural Engineering*, **137**(4): 481–491.
- Mazzoni S, McKenna F, Scott MH and Fenves GL (2006), *OpenSees Command Language Manual*, Pacific Earthquake Engineering Research (PEER) Center.
- Pan P, Wu SJ and Nie X (2015), “A Distributed Parameter Model of a Frame Pin-Supported Wall Structure,” *Earthquake Engineering & Structural Dynamics*, **44**(10): 1643–1659.
- Pan P, Zhao G, Lu XZ and Deng KL (2014), “Force–Displacement Mixed Control for Collapse Tests of Multistorey Buildings Using Quasi-static Loading Systems,” *Earthquake Engineering & Structural Dynamics*, **43**(2): 287–300.
- Qu Z, Wada A, Motoyui S, Sakata H and Kishiki S (2012), “Pin-Supported Walls for Enhancing the Seismic Performance of Building Structures,” *Earthquake Engineering & Structural Dynamics*, **41**(14): 2075–2091.
- Saatcioglu M and Razvi SR (1992), “Strength and Ductility of Confined Concrete,” *Journal of Structural Engineering*, **118**(6): 1590–1607.
- Zhao B, Taucer F and Rossetto T (2009), “Field Investigation on the Performance of Building Structures during the 12 May 2008 Wenchuan Earthquake in China,” *Engineering Structures*, **31**(8): 1707–1723.
- Zibaei H and Mokari J (2014), “Evaluation of Seismic Behavior Improvement in RC MRFs Retrofitted by Controlled Rocking Wall Systems,” *The Structural Design of Tall and Special Buildings*, **23**(13): 995–1006.